atoms

MDPI

Article

Magnetic Angle Changer for Studies of Electronically Excited Long-Living Atomic States

Łukasz Kłosowski * and Mariusz Piwiński

Institute of Physics, Faculty of Physics, Astronomy and Informatics, Nicolaus Copernicus University in Toruń, Grudziądzka 5, 87-100 Toruń, Poland
* Correspondence: lklos@fizyka.umk.pl

Abstract: A new geometry of a magnetic angle changer (MAC) device is proposed, which allows experiments to be run on electron impact excitation of long-lived states of target atoms. The details of the device's design are presented and discussed together with a numerical analysis of its magnetic field.

Keywords: backscattering; electron optics; inelastic collisions; numerical simulations

Citation: Kłosowski, Ł.; Piwiński, M. Magnetic Angle Changer for Studies of Electronically Excited Long-Living Atomic States. *Atoms* **2021**, *9*, 71. https://doi.org/10.3390/atoms9040071

Academic Editors: Jean-Christophe Pain and Grzegorz Piotr Karwasz

Received: 16 August 2021
Accepted: 23 September 2021
Published: 28 September 2021

1. Introduction

A magnetic angle changer (MAC) [1,2] was invented two decades ago as a device which allows the running of low-energy (below 100 eV) electron collisional experiments in the full range of scattering angles when a crossed-beam geometry is applied. Several various types of such devices have been used since then, allowing differential cross sections (DCS) and electron impact coherence parameters (EICP) to be obtained for numerous targets at various electron impact energies. A summary of such devices can be found in a review by G. King [3]. The most interesting devices worth mentioning are the MAC of M. Allan, using a single power supply [4], the MAC of B. Mielewska, providing zero magnetic field in the central part of the device [5], and the MAC of I. Linert providing a broad region of the homogeneous field [6].

Briefly, a MAC is a set of coaxial magnetic coils. Its total magnetic dipole moment is usually zero, providing negligible magnetic fields outside the device, which does not disturb electron beam sources or detectors of scattered particles. The device is symmetric, with a symmetry plane perpendicular to the main axis. The symmetry plane is transparent to electrons (no coils), identical to the experiment's scattering plane. The electron–target interaction region is placed in the central point of the MAC device.

The magnetic field of the MAC bends the electrons' trajectories in a way where the final direction is shifted by an angle defined by the electron's kinetic energy, the device's geometry, and electric currents flowing through its coils. This is very useful in experiments conducted at very large scattering angles, around 180°. Without a MAC, this would require placing an electron beam source (electron gun) and electron detector at the same angular position. If the MAC is used, electrons scattered at such large angles are deflected to a region where detectors can be physically placed.

Additionally, for inelastic scattering, the device can separate electrons scattered at 0° from the primary beam, allowing experiments to be run at very small scattering angles.

The magnetic field in the central region of the MAC (identical with the scattering region) is usually of the order of millitesla. Such a relatively weak field does not influence scattering processes significantly. It may, however, cause some issues in the interpretation of experimental results, especially in the EICP measurement.

The EICP can be defined as various sets of parameters describing the shape, orientation, and alignment of the electron charge cloud of collisionally excited atoms. More

details can be found in the review by Andersen et al. [7]. In the case of P states of two-valence-electron atoms, the most convenient EICPs are Andersen parameters P_l, γ and $L_\perp$ [8], defined as follows. An atom in its P state can be described as a superposition of three possible magnetic substates:

$$|P\rangle = a_{-1}|m=-1\rangle + a_0|m=0\rangle + a_{+1}|m=+1\rangle, \tag{1}$$

where a_{-1}, a_0, and a_{+1} are complex coefficients. Due to the planar symmetry of the scattering system, additional conditions for the coefficients appear. The mathematical form of these conditions depends on the choice of axes used to describe the atom. If a so-called natural reference frame is used, then such a condition is simply $a_0 = 0$. In such a frame, the quantization axis is perpendicular to the scattering plane defined by the momentum vectors of incoming and outgoing electrons. Equation (1) is then simplified to:

$$|P\rangle = a_{-1}|m=-1\rangle + a_{+1}|m=+1\rangle. \tag{2}$$

Then the angular part of electron cloud density in spherical coordinates (θ, ϕ) can be described using the expression:

$$|\Psi(\theta,\phi)|^2 = \frac{3}{8\pi}\sin^2\theta(1 + P_l\cos(2\phi - 2\gamma)), \tag{3}$$

where P_l is the shape parameter and γ is the alignment angle. They are related to the a coefficients (assuming normalization) with the expressions:

$$P_l = 2|a_{-1}a_{+1}| \tag{4}$$

$$\gamma = \frac{1}{2}\arg\left(-a_{-1}^* a_{+1}\right) \tag{5}$$

The third parameter $L_\perp$ is angular momentum transfer, and it is given with the expression:

$$L_\perp = |a_{+1}|^2 - |a_{-1}|^2. \tag{6}$$

Moreover, it is related to the shape parameter with the equation:

$$L_\perp^2 + P_l^2 = 1. \tag{7}$$

The geometrical interpretation of the parameters is presented in Figure 1.

In experiments on the EICP measurements in a weak magnetic field, an additional effect analogous to a well-known Hanle effect [9] is present, which was described in detail in the past [10,11]. The phenomenon was initially observed as a modification of the polarization state of light resonantly scattered by atoms placed in a magnetic field [12]. The effect finds numerous applications in atomic physics and astrophysics [13], and is used for example, to determine magnetic fields in laboratory plasmas [14] or in astronomical objects [15].

The Hanle-like effect we intend to avoid here is caused by the same mechanism in terms of quantum mechanics. The difference is that the atoms are excited not by resonant light, but by electron impact.

The presence of the magnetic field causes slight energy shifting in the atom's state, depending on the atom's magnetic dipole moment orientation and the magnitude of the field. For simplicity, we may assume that the magnetic field is parallel to the quantization axis in the considered reference frame. The energy shifts have opposite signs for both substates in Equation (2), causing a time-evolving phase shift between $|m=-1\rangle$ and $|m=+1\rangle$. This way, the charge cloud from Equation (3) will precess with Larmour frequency:

$$\omega = \frac{Be}{2m}, \tag{8}$$

where B is the magnetic field, e is the elementary charge, and m is the electron mass.

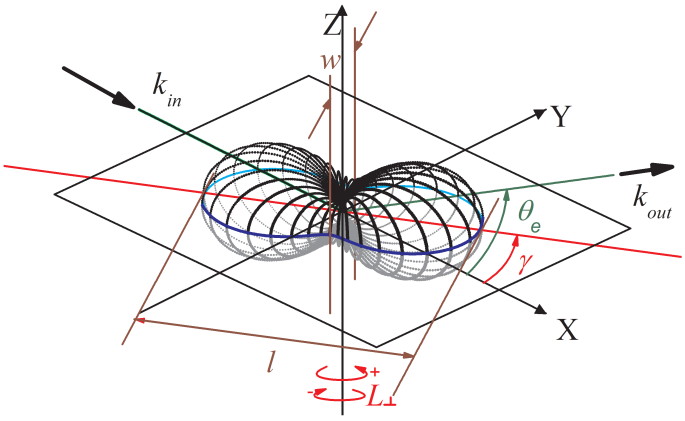

Figure 1. Geometrical interpretation of EICP. The 3-dimensional plot represents the angular part of the electron charge cloud in an atom's P state described with Equation (3). The value of $|\Psi|^2$ corresponds to the distance of the particular point of the surface from the center of the reference frame. The scattering plane is defined by the electron's initial and final wave vectors $\vec{k}_{in}$ and $\vec{k}_{out}$. The axes' orientation is chosen to form a so-called natural frame, where the quantization axis Z is perpendicular to the scattering plane. The electron is scattered at the angle θ_e. The alignment angle is denoted with γ. The shape parameter is given by the expression: $P_l = \frac{l-w}{l+w}$, where l and w are the length and width of the charge cloud, respectively.

Such a precession affects the measurement readout. The EICPs are usually studied using the electron-photon coincidence technique [16,17]. In such experiments, photons emitted from electron-impact excited atoms are detected. The information on EICP of the atom is written in the polarization state of the photon and in angular distribution of its emission probability. Such polarization or distribution can be determined experimentally.

There is a finite time interval between the collision act and photon emission, given by an exponential distribution described with the excited state's lifetime τ. This way, the precession of the charge cloud in the finite time leads to blurring the measurement results to $\tilde{P}_l$ and $\tilde{\gamma}$ values given with the expressions obtained by convolution of cloud rotation and exponential decay [10]:

$$\tilde{\gamma} = \gamma + \frac{1}{2}\arctan\frac{Be\tau}{m}, \tag{9}$$

$$\tilde{P}_l = \frac{P_l}{\sqrt{1+\left(\frac{Be\tau}{m}\right)^2}}. \tag{10}$$

It is worth noting that the magnetic field does not influence the angular momentum transfer $L_\perp$.

There are two ways of dealing with the problem of the MAC's field effect: One is to predict the effect's magnitude and include corrections in experimental data analysis, as was done in the e-Ca superelastic scattering experiment by the Manchester group [18]. Since Ca's 4^1P_1 state has a lifetime of 4.5 ns [19], then at 1 mT, the corrections are about 23° for γ and 0.69 for P_l, which are acceptable values.

The other way is to provide a near-zero magnetic field in the scattering region, allowing the Hanle-like effect to be reduced, as presented in our angular-correlation coincidence experiment on e-He scattering [10,20,21].

Both approaches are sufficient if the lifetime of the atomic state excited during the collision is short, of the order of a nanosecond. The situation becomes more complicated if the lifetime is longer, such as He 2^3P state's 98 ns [22]. In such a case, the corrections cannot be used, as the 1 mT field would blur the results of the shape parameter to 6% of its actual value, where the alignment angle cannot be determined well. On the other

hand, excitation to the triplet state is very interesting as one of few examples where we can observe purely spin-exchange collisions. The EICP for such scattering were measured only in a limited range of energies and scattering angles [23] and analyzed theoretically in only a few approaches [24,25].

Additionally, in the case of He's 2^3P state, a central-zero-field MAC would be useless, as the scattering region has finite dimensions, approximately 1 mm in diameter. The zero magnetic field is available only at the center of the MAC, but the field reaches up to 0.1 mT in outer parts of the finite region. This way, the Hanle-like effect of up to 30° would be observed in the outer layers of the scattering area. The experimental results would then include the magnetic field's effect averaged over the interaction region, which would be very difficult to deconvolve.

2. New Magnetic Angle Changer Geometry

To bypass the issues described above, a MAC of improved geometry can be used. It combines the features of three devices mentioned above (Allan's, Mielewska's and Linert's). Besides assuring zero magnetic dipole moment and zero magnetic field in the central region, it should also provide zero magnetic field in the center's vicinity. In other words, the magnetic field should be a homogeneous zero value in the whole scattering region.

To describe such a MAC, it is convenient to use cylindrical coordinates. The center of the device is the origin of the coordinate system, and the main axis is the system's Z axis. The position of each coil, denoted with index i, is then given with its radius r_i and distance from the symmetry plane z_i. Each coil transmits an electric current I_i (positive value for counterclockwise currents and negative for clockwise). For simplicity, one can assume the MAC is made of non-magnetic material with negligible magnetic susceptibility (copper in the experiment).

The zero magnetic moment condition is then fulfilled by the equation:

$$\sum_{i=1}^{N} I_i r_i^2 = 0, \tag{11}$$

where N is the total number of wire coils used in the MAC ($N = 30$ in the proposed design). The zero-field condition is fulfilled by the equation:

$$\sum_{i=1}^{N} \frac{I_i r_i^2}{\left(r_i^2 + z_i^2\right)^{\frac{3}{2}}} = 0. \tag{12}$$

To provide the homogeneity of the field, the second derivative of the magnetic field along the Z coordinate should be zero:

$$\frac{\partial^2}{\partial Z^2} \sum_{i=1}^{N} \frac{I_i r_i^2}{\left(r_i^2 + (z_i - Z)^2\right)^{\frac{3}{2}}}\Bigg|_{Z=0} = 0, \tag{13}$$

which leads to a condition, which is a generalization of a Helmholtz coil:

$$\sum_{i=1}^{N} \frac{I_i r_i^2 (r_i^2 - 4z_i^2)}{\left(r_i^2 + z_i^2\right)^{\frac{7}{2}}} = 0. \tag{14}$$

For simplicity of operation, it was assumed at the design stage that all the wires would be supplied with an electric current of the same value. Various geometries satisfy these conditions (11), (12), and (14). One of them was chosen for practical realization. The choice was made based on further numerical simulations of the electron beam's behavior. The selected MAC, among all the geometries we found, provided the best efficiency of bending the electron's trajectories and the lowest angular spread of the beam (see Section 2.2).

2.1. The Device Used in the Experiment

The cross section of the proposed MAC is presented in Figure 2, together with the produced field.

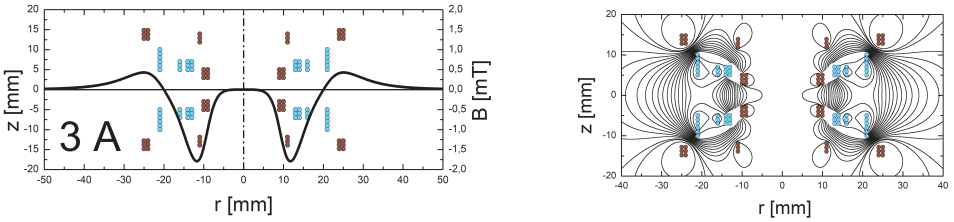

(**a**) (**b**)

Figure 2. The geometry of the proposed MAC coil. Panel (**a**) represents the cross-section through the wires. For clarity, the cores used to wind the coil are not shown. The colors of the wires indicate the direction of the electric current. Additionally, the magnetic field function at 3 A of the driving current is presented to show the wide field-free area in the central part of the device. The magnetic field was calculated numerically by integration of field contribution from all conductors using the Biot–Savart law. Panel (**b**) represents magnetic field lines in the cross-section of the MAC, also obtained from Biot–Savart.

The device consists of 30 pairs of circular wires arranged into coils. Details of their geometry are collected in Table 1.

Table 1. Collected information on the geometry of the MAC's coils. r_i refers to the radius of $i-$th coil, and z_i is its distance from the device's symmetry plane.

i	r_i [mm]	z_i [mm]	Current Direction
1	9	3	+
2	9	4	+
3	9	5	+
4	10	3	+
5	10	4	+
6	10	5	+
7	11	11.9	+
8	11	12.9	+
9	11	13.9	+
10	13	5	−
11	13	6	−
12	13	7	−
13	14	5	−
14	14	6	−
15	14	7	−
16	16	5	−
17	16	6	−
18	16	7	−
19	21	5	−
20	21	6	−
21	21	7	−
22	21	8	−
23	21	9	−
24	21	10	−
25	24	12.8	+
26	24	13.8	+
27	24	14.8	+
28	25	12.8	+
29	25	13.8	+
30	25	14.8	+

The device was set up using copper cores and 0.9 mm insulated copper wires. Such choice enables good heat transmission, essential for cooling at several amperes of operating current. Additional cooling was provided using a tap water system analogous to the one used with the previous MAC [10]. Photographs of the ready-to-use device are presented in Figure 3.

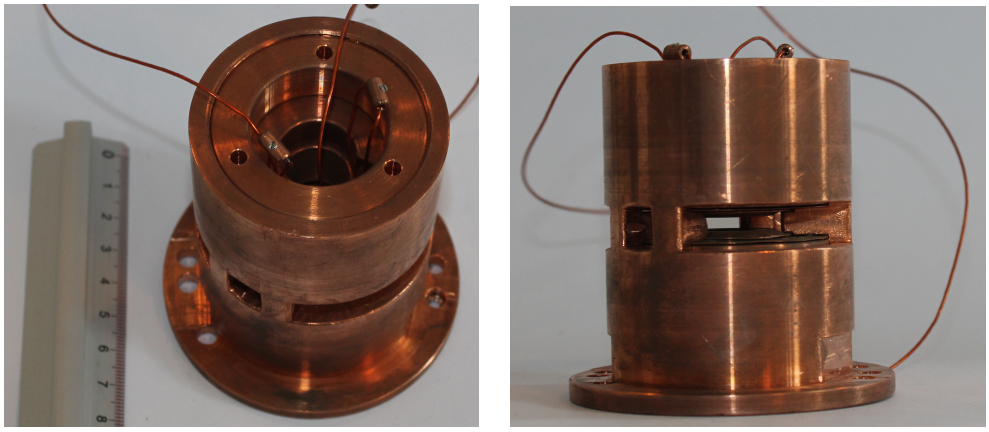

(**a**) (**b**)

Figure 3. Photographs of the MAC constructed based on the proposed design. Panel (**a**) shows the device's overview, with a ruler to indicate the size. Panel (**b**) shows the gap in the MAC's symmetry plane (scattering plane in the experiment). Some material is left in the gap to provide mechanical support of the upper part.

2.2. Numerical Analysis of the MAC's Performance

To prove the efficiency of the MAC, a set of numerical simulations was performed. Trajectories of electrons traveling through the device's field were calculated by integrating classical equations of motion using well-known Runge–Kutta methods with Lorentz forces and magnetic fields calculated from the Biot–Savart law, analogous to the method described in our previous works [10]. Example trajectories are presented in Figure 4.

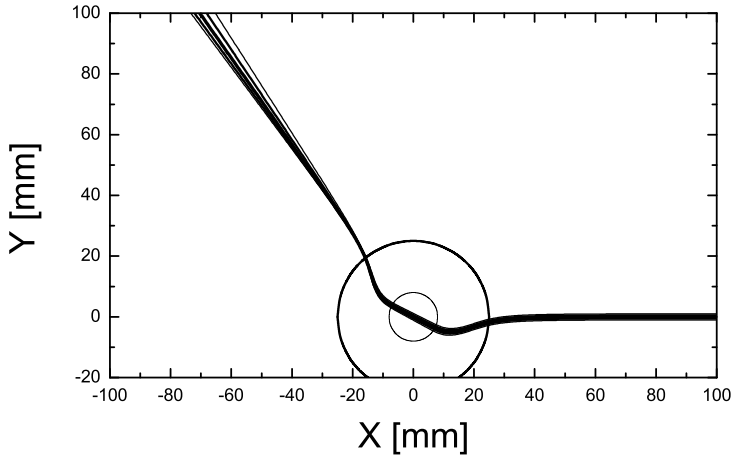

Figure 4. Example trajectories of electrons in the MAC's field obtained numerically at a 4 A coil current and 100 eV electron energy (projection in device's symmetry plane). The circle denotes the MAC's contour. The electrons are incoming from the right and are deflected up at about 50 degrees.

Similar simulations were repeated in various current and energy conditions for electron beams of 1 mm in diameter. This allowed us to determine the MAC's deflection efficiency and estimate the angular spread of the electron beam introduced by the magnetic field. The deflection angle ϑ of the electron's trajectory can be calculated numerically in

simulations, providing its nonlinear dependence from an expression $\frac{I_{MAC}}{\sqrt{E}}$, where I_{MAC} is the MAC's electric current, and E is the electron's kinetic energy. At low scattering angles, where the function is close to linear, such calculations can be simplified by using the approximate expression [10]:

$$\vartheta \approx \frac{2e}{\sqrt{2mE}} \int_0^\infty B(r)\mathrm{d}r \tag{15}$$

where e and m are the electron's charge and mass, and $B(r)$ is the magnetic field function, proportional to I_{MAC} (example presented in Figure 2a). Numerically obtained deflection angles are presented in Figure 5.

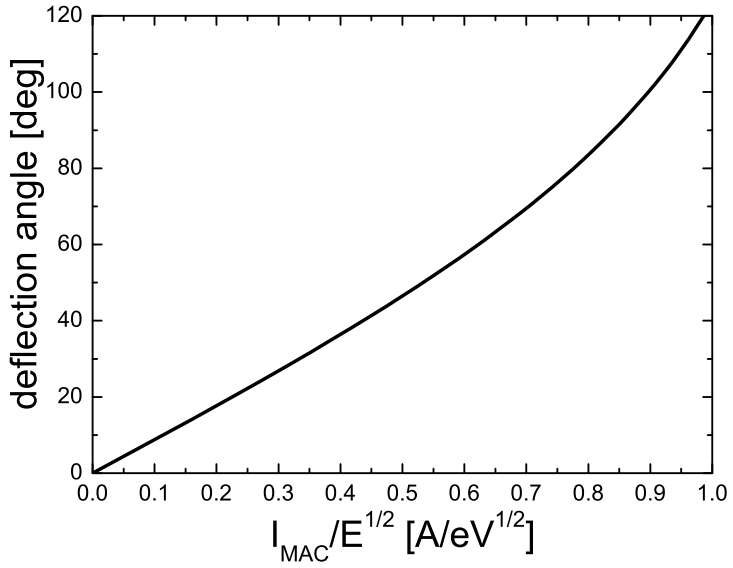

Figure 5. The deflection angle of electron trajectories obtained numerically. It is clear that at lower deflection angles, the linear function from Equation (15) provides a good approximation.

Additionally, since the magnetic field can cause some angular spread of the deflection angles, some additional simulations were performed for electron beams of finite width (1 mm in diameter). The estimated spread is presented in Figure 6.

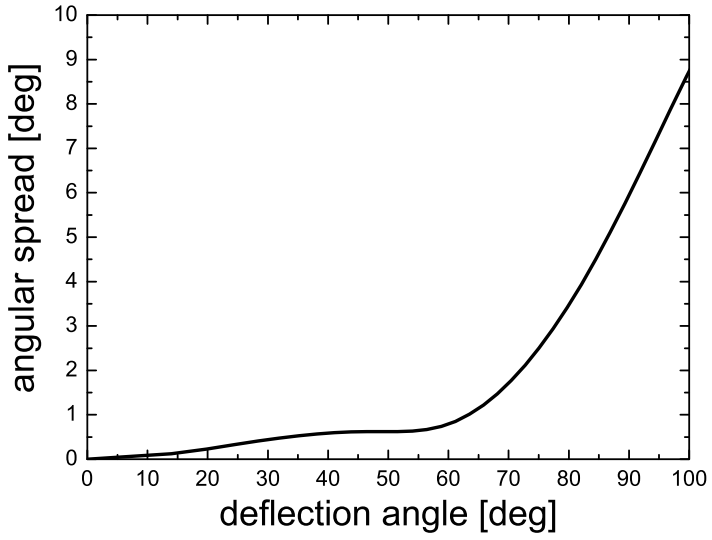

Figure 6. Numerically obtained angular spread of the electron beam introduced by the presence of the MAC's magnetic field.

It is clear that for deflection angles below 60 degrees, the angular spread is low and can be neglected for most electron scattering experiments, where beam divergences are usually greater than 1 degree. At deflection angles above 80 degrees, the spread grows rapidly, limiting the range of the MAC's use. On the other hand, the deflection of an electron beam of 60° is sufficient for most experiments involving backward scattering.

3. Summary

To summarize, a new, efficient magnetic angle changer was designed and built. Numerical analysis shows its efficiency for electron beams typically used in electron scattering experiments. The device can provide a near-zero, homogeneous magnetic field in its central part. It may allow experiments on electron impact coherence parameters to be run in the full range of scattering angles for atomic states with lifetimes close to 100 nanoseconds (such as the 2^3P state of the helium atom, as mentioned above), which will be the topic of further research of our group.

Author Contributions: Conceptualization, Ł.K. and M.P.; design of the device, Ł.K.; production of the device, Ł.K. and M.P.; numerical analysis, Ł.K.; preparation of the manuscript Ł.K. and M.P. All authors have read and agreed to the published version of the manuscript.

Funding: This research received no external funding.

Institutional Review Board Statement: Not applicable.

Informed Consent Statement: Not applicable.

Conflicts of Interest: The authors declare no conflict of interest.

References

1. Read, F.H.; Channing, J.M. Production and optical properties of an unscreened but localized magnetic field. *Rev. Sci. Instrum.* **1996**, *67*, 2372–2377. [CrossRef]
2. Zubek, M.; Gulley, N.; King, G.C.; Read, F.H. Measurements of elastic electron scattering in the backward hemisphere. *J. Phys. B At. Mol. Opt. Phys.* **1996**, *29*, L239–L244. [CrossRef]
3. King, G.C. Chapter 1-the use of the magnetic angle changer in atomic and molecular physics. In *Advances in Atomic, Molecular, and Optical Physics*; Arimondo, E., Berman, P.R., Lin, C.C., Eds.; Academic Press: Cambridge, MA, USA, 2011; Volume 60, pp. 1–64.
4. Allan, M. Excitation of the 2^3S state of helium by electron impact from threshold to 24 eV: measurements with the 'magnetic angle changer'. *J. Phys. At. Mol. Opt. Phys.* **2000**, *33*, L215–L220. [CrossRef]
5. Mielewska, B.; Linert, I.; King, G.C.; Zubek, M. Differential cross sections for elastic electron scattering in argon over the angular range 130°–180°. *Phys. Rev. A* **2004**, *69*, 062716. [CrossRef]
6. Linert, I.; King, G.C.; Zubek, M. A study of electron impact excitation of molecular oxygen at a scattering angle of 180°. *J. Electron Spectrosc. Relat. Phenom.* **2004**, *134*, 1–8. [CrossRef]
7. Andersen, N.; Gallagher, J.W.; Hertel, I.V. Collisional alignment and orientation of atomic outer shells I. Direct excitation by electron and atom impact. *Phys. Rep.* **1988**, *165*, 1–188. [CrossRef]
8. Andersen, N.; Hertel, I.V.; Kleinpoppen, H. Shape and dynamics of states excited in electron-atom collisions: A comment on orientation and alignment parameters by consideration of attractive and repulsive forces. *J. Phys. B At. Mol. Phys.* **1984**, *17*, L901–L908. [CrossRef]
9. Hanle, W. Zuschriften und vorläufige Mitteilungen. *Naturwissenschaften* **1923**, *11*, 690–691. [CrossRef]
10. Kłosowski, Ł.; Piwiński, M.; Dziczek, D.; Wiśniewska, K.; Chwirot, S. Magnetic angle changer—New device allowing extension of electron–photon coincidence measurements to arbitrarily large electron scattering angles. *Meas. Sci. Technol.* **2007**, *18*, 3801–3810. [CrossRef]
11. Murray, A.J.; MacGillivray, W.; Hussey, M. Theoretical modeling of resonant laser excitation of atoms in a magnetic field. *Phys. Rev. A* **2008**, *77*, 013409. [CrossRef]
12. Wood, R.W.; Ellett, A. On the influence of magnetic fields on the polarisation of resonance radiation. *Proc. R. Soc. London. Ser. Contain. Pap. Math. Phys. Character* **1923**, *103*, 396–403.
13. Moruzzi, G.; Strumia, F. (Eds.) *The Hanle Effect and Level-Crossing Spectroscopy*; Atomic, Molecular, Optical and Plasma Physics; Springer: Berlin/Heidelberg, Germany, 2012.
14. Presura, R. Hanle effect as candidate for measuring magnetic fields in laboratory plasmas. *Rev. Sci. Instrum.* **2012**, *83*, 10D528. [CrossRef]
15. Raouafi, N.E.; Riley, P.; Gibson, S.; Fineschi, S.; Solanki, S.K. Diagnostics of coronal magnetic fields through the hanle effect in uv and ir lines. *Front. Astron. Space Sci.* **2016**, *3*, L215. [CrossRef]
16. Bederson, B. The "perfect" scattering experiment. II. *Comments At. Mol. Phys.* **1969**, *1*, 65–69.

17. Macek, J.; Jaecks, D.H. Theory of atomic photon–particle coincidence measurements. *Phys. Rev. A* **1971**, *4*, 2288–2300. [CrossRef]
18. Hussey, M.; Murray, A.; MacGillivray, W.; King, G.C. Low energy super-elastic scattering studies of calcium over the complete angular range using a magnetic angle changing device. *J. Phys. B At. Mol. Opt. Phys.* **2008**, *41*, 055202. [CrossRef]
19. Available online: https://physics.nist.gov/PhysRefData/Handbook/Tables/calciumtable3.htm (accessed on 15 August 2021).
20. Kłosowski, Ł.; Piwiński, M.; Dziczek, D.; Wiśniewska, K.; Zubek, M.; Chwirot, S. Coincidence investigation of inelastic electron-atom collisions with magnetic selection of scattering angle—Feasibility study. *Eur. Phys. J. Spec. Top.* **2007**, *144*, 173–177. [CrossRef]
21. Kłosowski, Ł.; Piwiński, M.; Dziczek, D.; Pleskacz, K.; Chwirot, S. Coincidence measurements of electron-impact coherence parameters for e-he scattering in the full range of scattering angles. *Phys. Rev. A* **2009**, *80*, 062709. [CrossRef]
22. Available online: https://physics.nist.gov/PhysRefData/Handbook/Tables/heliumtable3.htm (accessed on 15 August 2021).
23. Humphrey, I.; Williams, J.F.; Heck, E.L. A feasibility study of the measurement of the stokes parameters of the 33p, 31d and 33d states of helium. *J. Phys. At. Mol. Phys.* **1987**, *20*, 367–391. [CrossRef]
24. Fon, W.C.; Berrington, K.A.; Burke, P.G.; Kingston, A.E. The 11s to 23s and 11s to 23p excitation of helium by electron impact. *J. Phys. At. Mol. Phys.* **1979**, *12*, 1861–1872. [CrossRef]
25. Cartwright, D.C.; Csanak, G. Electron-photon coincidence parameters for the excitation of the n3P (n = 2–8) states of helium *J. Phys. B* **1986**, *19*, L485–L491. [CrossRef]